Scintillations of star images observed through the atmosphere from onboard Salyut-7 and Mir space stations

G.M. Grechko,[1] A.S. Gurvich,[1] V. Kan,[1] S.A. Savchenko,[2] and A.I. Pakhomov[3]

[1] *Institute of Atmospheric Physics, Russian Academy of Sciences, Moscow*
[2] *Institute of Satellite Studies, Russian Academy of Sciences, Moscow*
[3] *Rocket-Satellite Corporation "Energy," Korolev, Moscow Region*

Received June 25, 2001

The results of observations of the star settings from onboard Salyut and Mir space stations in 1982–1993 with an EFO-1 photometer are summarized. The main purpose of these experiments was to study the small-scale structure of the inhomogeneities in density and temperature in the stratosphere from the measurements of stellar scintillations. A description of the measurement periods is presented, and a brief discussion of the measured results on the scintillation spectra is presented. The measurements with an EFO-1 have made it possible detection and study of the anisotropic inhomogeneities of the density of a stratified type. The estimates of the coefficient of the anisotropy inhomogeneity are obtained. The vertical spectra of density and temperature fluctuations in the stratosphere are retrieved. These spectra well agree with the results of *in situ* balloon-borne temperature measurements and modeling of saturated internal waves on the vertical scales from 0.1 to 1 km. The measurements have demonstrated the presence of characteristic vertical scale of the order of few meters in the vertical spectra of anisotropic temperature inhomogeneities in the stratosphere.

Introduction

The optical and radio transillumination of the planet and their satellites' atmospheres at occultation of natural and artificial sources of radiation have been among most promising methods of sensing the parameters and composition of the planet atmospheres. The advantages of this method, such as high accuracy and relative simplicity, have been successfully demonstrated in many experiments on radio transillumination of the planet atmospheres in solar system at occultation from the space stations and on the optical translucence in the ground-based astronomic observations of stellar occultation by the planetary atmospheres.[1,2]

The transillumination of the Earth's atmosphere in the optical range has been made on a regular basis using SAGE-II spectrometer[4] for studying the gaseous and aerosol composition of the atmosphere from extinction measurements. In these experiments, the entrance slit of the spectrometer cut only part of the solar image, so that the solar flux passed through the spectrometer slit did not suffer from the refraction effect.[5] To study the refraction of light from onboard a satellite, the photographing and filming of sunrises and sunsets[3] and observations of stellar scintillation were performed. In photographing and filming of the entire sun disk, the refraction results in a regular oblation of the sun disk and in random deformations of the sun disk contour.

Unlike the sun, the stars, when setting behind the Earth's atmosphere and observed from the satellite, are not resolved by the receiving instrumentation, so they can be regarded as point-like sources. The air density regularly decreases with height in the atmosphere (and so, does the refractive index), analogous to the action of a negative lens, which leads to a regular attenuation of light flux coming to the entrance aperture. The random inhomogeneities of the density – weak focusing and defocusing "lenses" – lead to random variations of the measured light flux, or scintillations. Due to a rapid, almost exponential decrease of the air density with height, the main contribution to scintillations comes from the inhomogeneities localized in the region near the perigee of the beam, and the sizes of this region are much less than the distance between it and the receiving satellite. Since the satellite has quite high velocity, the frozen density distribution hypothesis does work to convert the statistical characteristics of the observed time realizations to the spatial ones.[6]

From these characteristics, it is possible to calculate the corresponding statistical characteristics of the inhomogeneities in the refractive index n or refractivity $N = n - 1$ of the air. In the optical range, relative fluctuations of the refractive index are equal to the relative fluctuations of the air density or, with an opposite sign, to the relative fluctuations of temperature when the pressure fluctuations are neglected. The characteristics of the density fluctuations are calculated from the data of scintillation measurements, based on the theory of light propagation in the randomly inhomogeneous media. For the satellite occultation experiments, a convenient and frequently used approximation is the approximation of an equivalent phase screen, approximating the effect of the atmosphere on radiation propagated through it. The validity of this approximation is based on the following facts: (1) as was already noted above, the scintillations are determined by a relatively small region in the atmosphere near the beam perigee and, beyond, the light can be assumed to propagate in a free space; and (2) for the beam perigee heights over 15–20 km, the scintillations at top of the

0235-6880/01/12 1026-12 $02.00

atmosphere are small and increase outside of the atmosphere in the free space.[7] In this case, under conditions of weak-oscillations (when the scintillation index is less than 1), the scintillation spectrum can simply be related to the three-dimensional spectrum of the refractive index fluctuations in the atmosphere.[7–10,15]

In 1982 at the Salyut-7 orbital station, the observations of stellar scintillations through the atmosphere were initiated to be performed with the use of EFO-1 photometer,[11] aimed at studying the fine structure of the air density in the stratosphere. The operation of Salyut-7 station stopped in 1986, but before this happened the EFO-1 photometer had been moved to the Mir station where it remained operated until 1993. The main results of analysis of EFO-1 data are detailed elsewhere.[11–22] Here, we present only a brief summary of the many-year experiments with the EFO-1 photometer. The paper presents a general characterization of the observations and the main parameters of the experiments, as well as some results unpublished earlier, and the relationships and specific features in the observed stellar scintillations. Also, the primary purpose is to summarize the main results, published separately, in one paper and provide a modern insight into them now, 15 years after their first publications. In addition, an attention will also be given to the anomalous facts from the viewpoint of standard atmosphere; these facts were recorded earlier by the crews of the spaceships, but not published yet.

The observations performed with a EFO-1 photometer, enabled not only obtaining a series of interesting results, but also to formulating main requirements to the development of a new specialized photometer for observations of the stellar scintillations, that were fruitfully incorporated in designing the EFO-2 instrument.[23–25]

1. EFO-1 photometer. Description of observations

The photometer EFO-1 was developed by I. Zakharov and L. Neuzhil from the Astronomical Institute of Czechoslovakian Academy of Sciences.[11] It was designed primarily to determine, from attenuation of radiation from the stars during their set, the optical density, sizes, and time variations of the layer formed due to burning meteorites at about 100 km heights.

After refinement, aimed at extending the frequency band of analog amplifiers of a receiver to 100 Hz, the device can now be used to observe the stellar scintillations caused by the refractivity fluctuations, when rays in the atmosphere pass at heights from 40–45 down to 15 km. The diameter of the receiving objective of the photometer is 90 mm and its focal length is 500 mm. The field of view (FOV) of the measurement channel is 10 minutes of arc and that of the visual channel is about 3°.

As a detector we used a Tesla GIPK-50 photomultiplier with a S-11 super photocathode, followed by an amplifier; the photocurrent (sensitivity) was regulated by varying the voltage applied to the cathode. In the photometer, the allowance is made for using filters, centered at the maximum of quantum efficiency of the photocathode at a wavelength of 450 nm: narrowband filter F_1 with the full width at half-maximum (FWHM) of 50 nm and filter F_2 with the FWHM of 180 nm; as well as a reception of a signal without a light filter in an open window of the filter holder. The photometer was assembled at the illuminator of an orbital station on a gimbal, using which a crew could perform manual aiming and tracking of the stars.

At the beginning of each measurement series, the sensitivity adjustment of the detector was performed using a pre-selected star when it was at extraterrestrial heights of the ray perigee over 100 km. The star-induced photocurrent measurement during obscuration of the star by the atmosphere was performed from the heights about 100 km down to heights of approximately 15 km, until an observer lost the star due to attenuation of light in the atmosphere. We recorded the values of photocurrent and the voltage applied to the photocathode as the output telemetry data. The dynamic range of the data was chosen to be 256 levels, in accordance with the capabilities of the telemetry system. In order to gain maximum possible altitude coverage, in detector sensitivity adjustment the mean level of the star-induced vacuum photocurrent was chosen to be approximately 0.5–0.7 of the upper limit of the dynamic range, ensuring a reduction of strong signal surges. For each measurement series, we calculated ballistic data as a function of time: coordinates and velocity of orbital station, and coordinates of the ray perigee and its height in the atmosphere. In calculating the ray perigee h_p, a standard atmospheric model was used to take into account the atmospheric refraction.

The effective atmospheric thickness along the line-of-sight path is few hundred kilometers, while the distance from the perigee to the orbital station is about 2100 km. Depending on how satellite orbital pole is oriented with respect to the direction toward the star, different star movement trajectories can be realized in the perigee plane (the plane normal to the ray and passing through the perigee point). From the observations at different viewing geometries, one can sense the atmosphere along different directions, from vertical $\alpha = 0°$ to horizontal $\alpha = 90°$, where α is the angle between line tangential to the projection of the star trajectory onto the perigee plane and local vertical. To minimize the shot noise effect in a photomultiplier, the observations were made of the brightest stars.

Part of the observations was made using light filters. Despite the visual reduction of the received radiative flux and enhanced noise, this, on the other hand, yielded a reduction in the chromatism due to the refraction in the atmosphere. This effect is essential in the fact that, because rays with shorter wavelengths experience stronger refraction in the atmosphere, differently colored rays, arriving from different heights h_p, will come simultaneously to the observation point.

The characteristic scale of the chromatic ray spacing in the vertical Δh_c depends on the radiation bandwidth of the incoming flux and height h_p. The effective spectrum of radiation is determined by the spectral characteristics of radiation from the star, transmission of the atmosphere, light filter, and quantum efficiency of a photomultiplier. Because of the asymmetry (due to chromatism, the rays are spaced only in vertical), this causes different effects on the scintillations due to isotropic and anisotropic inhomogeneities for different viewing angles. For a more detailed description of how chromatism influences the scintillations, see the section analyzing the spectra of scintillations (and also consult Ref. 25). In particular, during vertical star sets, averaging of received signal over altitude scale Δh_c leads to smoothing of the small-scale oscillations. The chromatism (which is the stronger, the wider the wavelength band of received radiation and the lower the sensing height) is insignificant for scintillation observations with EFO-1 device at high altitudes $h_p > 35–40$ km, but it becomes a dominating factor at lower altitudes.

The Table below lists 47 observation series analyzed out of the total number performed during 1982–1993.

Table. Measurement series

Case No.	Date	Orbit No.	Source	m_v	Coordinates of perigee		f_s, kHz	Filters	α, degrees
					N	E			
1	10.30.82	–	Deneb	1.26	2	173	0.003	F_1	–
2	10.30.82	–	Vega	0.04	20	159	0.003	F_1	–
3	10.30.82	–	Arcturus	−0.06	57	110	0.003	F_1	–
4	11.05.82	–	Deneb	1.26	−14	133	0.012	0	–
5	09.11.85	9591	Arcturus	−0.06	65	97	1.6	0	56.1
6	09.21.85	9743	Vega	0.04	−11	218	0.16	0	34.3
7	09.21.85	9744	Vega	0.04	−11	195	0.16	0	34.2
8	09.21.85	9746	Saturn	0.8	22	123	0.16	0	82.1
9	09.21.85	9747	Saturn	0.8	23	99	0.16	0	82.8
10	11.06.85	0470	Arcturus	−0.06			1.6	0	86.3
11	10.05.87	9350	Achernar	0.53	32	113	1.3	0	86.54
12	10.06.87	9366	Achernar	0.53	32	103	1.3	0	87.47
13	10.08.87	9397	Arcturus	−0.06	69	105	1.3	0	–
14	10.08.87	9398	Arcturus	−0.06	70	85	1.3	0	85.72
15	10.09.87	9413	Arcturus	−0.06	69	101	1.3	F_2	84.54
16	11.25.87	0158	Canopus	−0.73	34	155	1.3	F_1	82.9
17	02.02.88	1244	Canopus	−0.73	34	132	1.3	F_1	80.9
18	02.02.88	1246	Canopus	−0.73	34	87	1.3	F_1	81.52
19	02.03.88	1260	Canopus	−0.73	34	125	1.3	F_1	83.0
20	02.03.88	1261	Canopus	−0.73	34	102	1.3	F_1	83.28
21	02.03.88	1262	Canopus	−0.73	34	79	1.3	F_1	83.16
22	02.04.88	1275	Canopus	−0.73	34	141	1.3	F_1	83.95
23	02.04.88	1276	Canopus	−0.73	34	118	1.3	F_1	84.0
24	02.04.88	1277	Canopus	−0.73	34	95	1.3	F_1	84.05
25	02.05.88	1291	Canopus	−0.73	34	135	1.3	F_1	85.56
26	02.05.88	1292	Canopus	−0.73	34	112	1.3	F_1	85.77
27	02.05.88	1293	Canopus	−0.73	34	89	1.3	F_1	85.88
28	04.04.88	2223	Sirius	−1.43	45	117	1.3	0	55.42
29	04.04.88	2224	Sirius	−1.43	45	96	1.3	0	59.54
30	04.05.88	2238	Sirius	−1.43	44	137	1.3	F_1	62.94
31	04.05.88	2239	Sirius	−1.43	43	114	1.3	F_1	62.94
32	04.05.88	2240	Sirius	−1.43	43	91	1.3	F_1	63.82
33	04.05.88	2241	Sirius	−1.43	43	68	1.3	F_1	63.87
34	04.06.88	2254	Sirius	−1.43	42	132	1.3	F_1	64.91
35	02.28.89	7416	Capella * (22.8 km)	0.09	−10	276	0.146	F_1	–
36	02.28.89	7417	Capella * (29.8 km)	0.09	−10	244	0.146	F_1	–
37	02.28.89	7418	Capella * (37.0 km)	0.09	−10	221	0.146	F_1	–
38	11.19.89	3542	Achernar * (11.8 km)	0.53	30	101	1.3	0	–
39	11.19.89	3543	Achernar * (12.6 km)	0.53	30	76	1.3	0	–
40	08.06.91	3299	Vega	0.04	−12	295	0.146	0	87.0
41	08.06.91	3300	Vega	0.04	−11	273	0.146	0	87.3
42	08.16.91	3459	Canopus	−0.73	5	231	0.146	0	86.8
43	08.16.91	3460	Canopus	−0.73	4	206	0.146	0	86.7
44	10.19.92	2157	Canopus * (35.0 km)	−0.73	23	306	1.0	0	–
45	10.19.92	2158	Canopus * (29.8 km)	−0.73	23	282	1.0	0	–
46	12.16.93	762	Canopus * (46.8 km)	−0.73	24	146	1.3	0	–
47	12.16.93	763	Canopus * (51.8 km)	−0.73	25	123	1.3	0	–

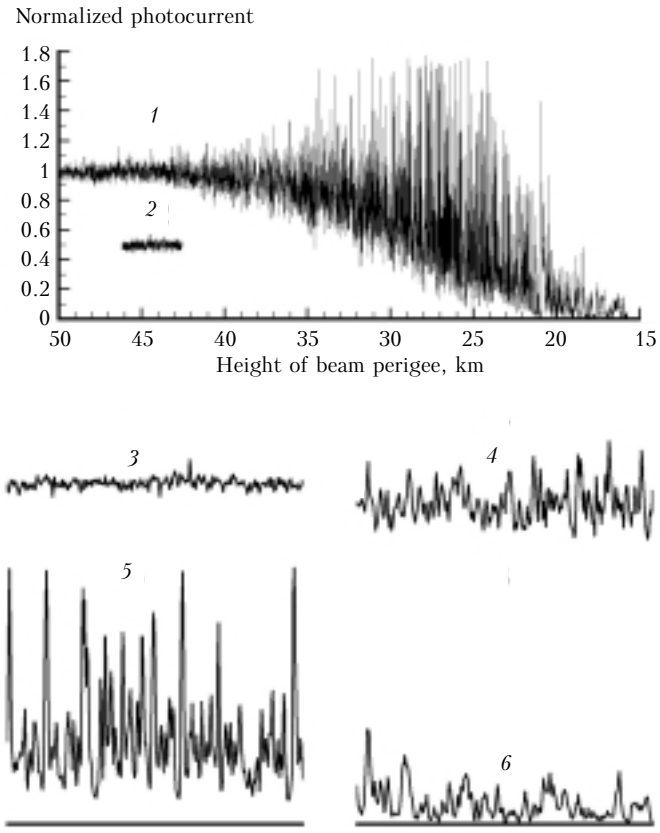

Fig. 1. Photocurrent record: photocurrent normalized to its extraterrestrial value during set of Canopus in measurement series No. 21 (curve *1*); shot noise (curve *2*); sections of realizations of photocurrent record (curves *3*–*6*): height 46–47 (*3*), 35–36 (*4*), 26–27 (*5*), 19.5–20.5 km (*6*).

The first 10 series were performed at Salyut-7 orbital station, and the remaining ones at the Mir orbital station. The star brightness is given in units of stellar magnitude m_v, and f_s is the signal sampling rate. The coordinates of the perigee point and the angles α are given for the perigee height of 30 km. In the column with the star names, asterisks show the series in which the star was observed at angles $\vartheta \le 18°$ from the orbital pole. In such observations, the star did not set below the Earth's horizon at all; but rather, after reaching a minimum height h_{min} (given in parentheses), it then rose again. For these series, the perigee coordinates are provided for the region with h_{min}. Observations made without filters are indicated by 0.

From the data presented above it is seen that the measurements cover all seasons, the latitude of the sub-perigee point varies from 11°S to 70°N, and the underlying surfaces range from the ocean to mountain systems. The measurements were made for different viewing geometries, with the star set angles α from 35 to 90°.

2. Method of data processing

As an example, Figure 1 shows a photocurrent recorded during a set of Canopus on February 3, 1988 (case 21 in the Table). The abscissa axis shows the ray perigee height, while the ordinate axis shows the values of the photocurrent normalized to its extraterrestrial value. Also shown in the same figure is a fragment of the record of shot noise of 4-s duration obtained at height h_p near 100 km, and below are some fragments of the record corresponding to the height difference of 1 km. In this measurement series, the wavelength range of received radiation was determined primarily by the transmission band of the filter F_1 used. As the star sets, the mean signal level decreases, leading to appearance of the atmospheric scintillations. For instance, at h_p = 46–47 km (case *3*), the rms values of scintillations are comparable with the rms values of shot noise in the measurement frequency band. As the ray path descends through the atmosphere further on, the scintillations grow (case *4*), until reaching their maximum at the heights about 25 km (case *5*). In this region, we had restricted separate strong signal outbursts because of insufficient dynamic range of the telemetry. The influence of chromatism due to the refractivity can be visually seen in Fig. 1 from smoothing of high-frequency scintillations, most evident in case *6*.

The case considered above shows a typical pattern of the high-frequency (small-scale) scintillations on random inhomogeneities in the refractive index, with the peaks of a strong signal exceeding considerably not only the mean intensity, but also its vacuum value, and with deep signal fading. This is because scintillations

caused by the atmospheric turbulence are determined by the smallest-scale inhomogeneities in the refractive index (in the geometric optics approximation, by the second derivative of correlation function of the refractivity fluctuations[26]). On the other hand, depletion of signal, associated with atmospheric attenuation, i.e., with the molecular and aerosol scattering and absorption, is determined by the distribution (rather than by the derivative of this distribution) of the concentration of absorbing components over the ray path; therefore, the extinction effects are the stronger, the greater the scales of these components. In addition, the scattering and absorption lead only to attenuation of radiation coming to the receiver; while, as seen from the Table, the random refraction also leads to random focusing/ /defocusing effects. On account of this fact, it was assumed that high-frequency (small-scale) structure of the measured signal, with the vertical scales on the order of kilometer or less, is caused by random fluctuations in the field of the refractive index; while the components of the atmospheric attenuation contribute to regular (mean) signal variation with a characteristic scale of a few kilometers or more in vertical.

The altitude of the measured scintillations was determined using ballistic data with the subsequent correction with respect to some mean transmission at some reference altitude, chosen to be 30 km in our case. For this, the measured profiles of the mean transmission were shifted in time until complete coincidence of the measured transmission at the height of 30 km with the value calculated from standard atmospheric model is achieved. The error in absolute determination of measurement time could be a few seconds in separate measurement series.

In the data processing, the main attention was paid to calculation of the scintillation spectrum. The frequency spectra of scintillations were calculated by means of fast Fourier transform using fragments of the realization corresponding to the altitude interval 3–4 km. Thus obtained estimates were then smoothed within a rectangular window with a constant quality factor $Q = 2$. To control the frequency response characteristic of the receiving system, we calculated the spectra of shot noise, representing, once appropriately normalized, the coefficient of direct power transfer of the entire receiving system. This transfer characteristic was used for correction of scintillation spectra at high frequencies, up to 100 Hz.[14] In addition, the spectra of shot noise were used for subtracting the noise contribution from measured photocurrent fluctuation spectra to obtain the proper scintillation spectra.

The frequency spectra of scintillations were recalculated to the one-dimensional spatial spectra under assumption that the spatial distribution of the refractivity field remains "frozen" over the measurement times. For scintillations, a significant parameter is the velocity of motion of the perigee point in the direction perpendicular to the ray path. The length of the realization fragment used determines the upper bond to the scintillation scales. The lower bond is determined by the net effect of the following factors: shot noise, upper bond of the frequency response of the detector, and chromatism.[14]

3. Mean atmospheric transmission

Figure 2 presents the mean photocurrents for 12 series of measurements, performed using filter F_1: cases 16, 18, 20, 21, 25–29, and 31–34. The averaging was performed over 2-s intervals for star sets with $\alpha > 80°$ and over 1-s intervals for the sets with $\alpha < 65°$. The corresponding vertical averaging scales changed from 2 to 1 km with the decreasing height. Bold dashed line shows the altitude profile of the transmission, calculated using a standard atmosphere model; it is caused by regular aerosol scattering and ozone absorption in the Chappuis band.[27] From Fig. 2 it is seen that the measured profiles of the mean transmission do agree, reasonably well, both with each other and with the data calculated using a model of standard atmosphere at the corresponding wavelength, a good sign in support of the method of correction of measurement altitude determination used here.

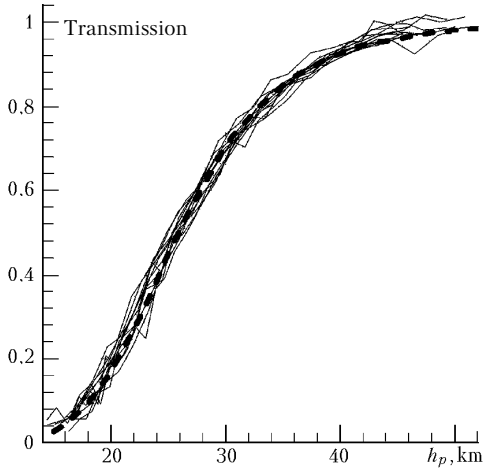

Fig. 2. Mean atmospheric transmission. Bold dashed line shows data calculated using model of a standard atmosphere.

However, considerable deviations in the behavior of the mean transmission were observed in some cases, which cannot be explained in the framework of standard atmospheric models. In some cases, these anomalies could not only be attributed to certain atmospheric phenomena, but also studied. For instance, in August 1991, i.e., two months after Pinatubo eruption, a series of measurements was performed (cases 40–43) to study attenuation of light by the stratospheric aerosol cloud in the tropics. These observations are used to estimate the vertical optical depth of the volcanic cloud and to study the fine vertical structure of the cloud.[20] In cases 17 and 22, the measurements of the mean signal level were contaminated by scattered light from the Moon, falling within the photometer measurement channel. This illumination grew with the increasing air density; it had been marked starting from approximately 30 km,

and rapidly increased from height of 20 km downward. In the case No. 10, star tracking was made against the background of auroras.

In case 6, for ray perigee height of 20 km, a rapid decrease of signal level (down to 0, according to telemetry records) was observed for approximately 2 s. In this case, the star set was observed by two spacemen simultaneously, using an EFO-1 photometer and a wider-FOV brightness amplifier.[13] The star image on the screen of the amplifier was filmed by a camera. A dip in the signal from the star was simultaneously recorded in independent observations. Detailed characteristics of the dip (duration, amplitude, and shapes of the front edge and the tail) consistently agree between the two cases, suggesting that it is not an artifact due to operator or instrumentation error, and caused by an isolated aerosol formation in the atmosphere. As estimates show, the vertical size of this cloud, located at the height about 20 km, was approximately 2 km, while the integrated optical depth along the ray path was more than an order of magnitude larger than the background level.

Most common anomalies presented in the Table are short-term signal fadings (for a constant photometer sensitivity) with the amplitude from a few percent of the mean level out to complete signal vanishing. The character of these dips, their shapes, and altitudes at which they were observed all strongly vary. However, it can be noted that they generally have steep fronts with the duration of 0.1–0.5 s; lower-amplitude dips having usually smaller duration. Possibly, these dips are the results of short-term star losses in measurement channel during star tracking. Favoring this is the fact that the dip duration is close to the characteristic time of the operator response, and that, provided the spaceman had already made a series of sequential observations, the newer observations had fewer dips than the older ones.

Besides, there are dips with long duration; for instance, in the case 23, at height 73 km, a slow decrease of the mean signal level occurred in the record, with the duration of 2.5 s and amplitude of 5%, followed by a rapid recovery. Possibly, a slow drift of the light spot across the photocathode, during the star tracking, causes this behavior, as the photocathode surface has nonuniform sensitivity, followed by a rapid return of the star image back to the FOV center performed by a spaceman.

As separate events, there are wavelike variations in the mean signal level at heights of 47–50 km in case 19, unlikely to be due to imprecise star tracking. There are three periods: the first one has the modulation amplitude in the full swath of approximately 50% of the mean level with the duration of 1 s, which corresponds to height difference of 2 km; whereas the other two periods have amplitudes of 30 and 20% and duration of 0.5 s. At the same time, the voltage applied to the cathode of the photomultiplier remained constant to within a quantum of telemetry. For this period, the coordinates of the orbital station were 52°N and 130°E, while coordinates of perigee were 34°N and 123°E, which eliminates the possibility of stray light from auroras. Such a wide range of signal variations cannot be explained by the modulation of nighttime sky illumination, since the flux from such a bright star as Canopus is many times higher than the signal level from illumination in the FOV of photometer measurement channel. In the next orbit, in case 20, no such signal variations were observed. A similar wavelike pattern in the mean signal level, but a weaker one, was also observed in the case No. 46 at the height of 150 km with the duration of 7 s (altitude difference of 3 km) and amplitude of approximately 5%.

4. Character of scintillations

Because, as will be shown below, the observed scintillations were mostly caused by anisotropic stratified inhomogeneities, in observations with large star set angles α the characteristic frequencies of scintillations are shifted toward lower values, leading to a decrease of the vertical component of the shift velocity of the perigee point. Besides, the amplitude of scintillations increased, while their variance remained unchanged, as the frequency range became narrower.

In each measurement series we observed the excursions of the parameters, characterizing the scintillations, from their means, and the spread of parameters could be considerable. Some quantitative characteristics of the altitude dependence of scintillations and scintillation spectra, as well as the scintillation dispersion, are analyzed in Ref. 19, here we only note the following characteristic heights, obtained using the entire data base:

– start of scintillations (discernible against the noise background) at 45–50 km;

– marked intensification of scintillations at 35–40 km;

– strong spikes and deep dips at 23–32 km;

– isolated spikes at 20–25 km;

– end of observations (loss of the star) at 13–15 km.

In a number of observations, localized regions with "spikes" of scintillations were observed at heights of 50–55 km, associated with intermittency of turbulence in the atmosphere. The intermittency effect manifests itself more clearly at higher altitudes because, seemingly, it is more characteristic of those altitudes, and also because at the lower altitudes the intermittency effect is masked by the higher level of scintillations.

The rms values of scintillations, the scintillation indices, in the region of weak fluctuations (up to the heights of 25–30 km) in the first approximation increase nearly exponentially during a star setting with the scale equal to the height of homogeneous atmosphere (6–7 km) at these altitudes. We note that the characteristic altitudes mentioned above have considerable variance comparable with this scale. It should be stressed that these altitudes and their spread are caused not only by the atmospheric turbulence (which depends on season, observation region, etc.), but also by (1) the

parameters of an EFO-1 photometer used: its sensitivity as well as frequency and dynamic ranges, and (2) by the observation conditions such as brightness and spectral characteristic of the star, viewing geometry, and wavelength range of the received radiation. The latter factor, in particular, determines the effects of chromatism in the atmosphere.

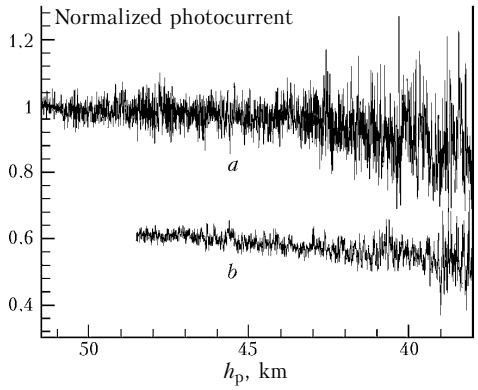

Fig. 3. Normalized photocurrent obtained in case 39 during (*a*) star rise and (*b*) star set. The record (*b*) is shifted by 0.4 downward.

The variability of scintillations over different observation regions is most clearly seen from observations of star set or star rise in a single orbit, as well as in the adjacent orbits. Most clear example of such variability of scintillations is presented in Fig. 3, which shows photocurrent records obtained during star set and star rise. The time series are for the altitude range 38–51 km, in which the variations between the scintillations are most clearly seen; they are shifted in time by approximately 10 min. The observations in this measurement series were performed without a filter, which allowed us to record scintillations at large altitudes. The coordinates of perigee point for the middle of the presented records were 31.5°N, 53.0°E during star set and 24.0°N, 96°E during star rise. As seen, the scintillations in the region of star set were much stronger (the level of shot noise can be deduced from the portion of the record (*b*) for altitudes higher than 45 km). Comparison with the data of observations during previous orbit (case 38) also indicates that the record (*a*) has an increased level of scintillations. As analysis of scintillation spectra shows,[18] a strong increase of fluctuations in the record (*a*) was also accompanied by qualitative changes in scintillation spectrum, with increased level of high-frequency scintillations.

It is also worth noting the scintillation anomalies observed in case 47. In this observation, the star was observed near orbital pole with h_{min} = 51.8 km. In the region of the star set near h_{min} at heights between 54 and 52 km, for 500 km in horizon, scintillations with the anomalously high level were recorded. Analysis of variations of the refractive attenuation at these altitudes has revealed thin (with the vertical sizes 50–200 m) regions with very strong vertical variations in temperature. Calculations of these inhomogeneities in the spherical symmetry approximation have shown that the temperature gradient in these layers may reach from 4 to −7 K/100 m.[21]

5. Scintillation spectra and anisotropy of the inhomogeneities

Stable temperature stratification, characteristic of the stratosphere, leads to a suppression of the vertical motions and favors the development of anisotropic, horizontally elongated inhomogeneities. Such anisotropic inhomogeneities arise during propagation of internal gravity waves.[28]

By sensing the atmosphere at different viewing angles α it is possible to study the anisotropy of inhomogeneities of the density in the atmosphere, assuming their symmetry in the horizontal plane. By inhomogeneity anisotropy coefficient, η, we will mean the ratio between the characteristic horizontal and vertical inhomogeneity scales. Qualitative conclusions can be drawn from comparative analysis of scintillation records themselves; but more obvious results can be derived from analysis of one-dimensional spatial scintillation spectra V_I, obtained for different α. If the density inhomogeneities are statistically isotropic, then the scintillations do not depend on direction, along which the rays cross these inhomogeneities. Hence, the scintillation spectra must coincide after they are recalculated as a function of wave numbers $\kappa_\perp$ along the visible star set trajectory in the perigee plane; here $\kappa_\perp = 2\pi f/v_\perp$, with f the frequency, and $v_\perp$ the perpendicular component of shift velocity of perigee point. However, if the inhomogeneities are strongly anisotropic, then the characteristic scintillation frequencies must be determined by vertical shift velocity of the perigee point v_v. In this case, the scintillation spectra must coincide after their recalculation to functions of vertical wave numbers $\kappa_v = 2\pi f/v_v$.

Figure 4 presents spatial scintillation spectra for 5 observation periods in the form of dimensionless products $\kappa_\perp V_I(\kappa_\perp)$ and $\kappa_v V_I(\kappa_v)$ for two altitude ranges. For these measurements, $\cos\alpha$ differs by almost a factor of ten (see the Table). The velocities $v_\perp$ and v_v differ correspondingly. For statistically isotropic inhomogeneities, the spectra $\kappa_\perp V_I(\kappa_\perp)$ must be closer for star sets with different $\cos\alpha$. For anisotropic inhomogeneities, this is the case for the spectra $\kappa_v V_I(\kappa_v)$.

In Figs. 4*a* and *c*, the spectra differ by approximately an order of magnitude along the axis of spatial wave numbers $\kappa_\perp$. At the same time, the scintillation spectra in Figs. 4*b* and *c*, reduced to the case of vertical sensing, reasonably well agree in shape. Some of the existing differences among them (primarily in terms of the spectral amplitudes) most likely result from the difference in altitudes for which they were calculated. From such a comparison, a lower bound for anisotropy coefficient η can be estimated as the ratio of horizontal to vertical ray shift velocity. As an example, such an estimate for the case No. 12 gives $\eta > 25$.

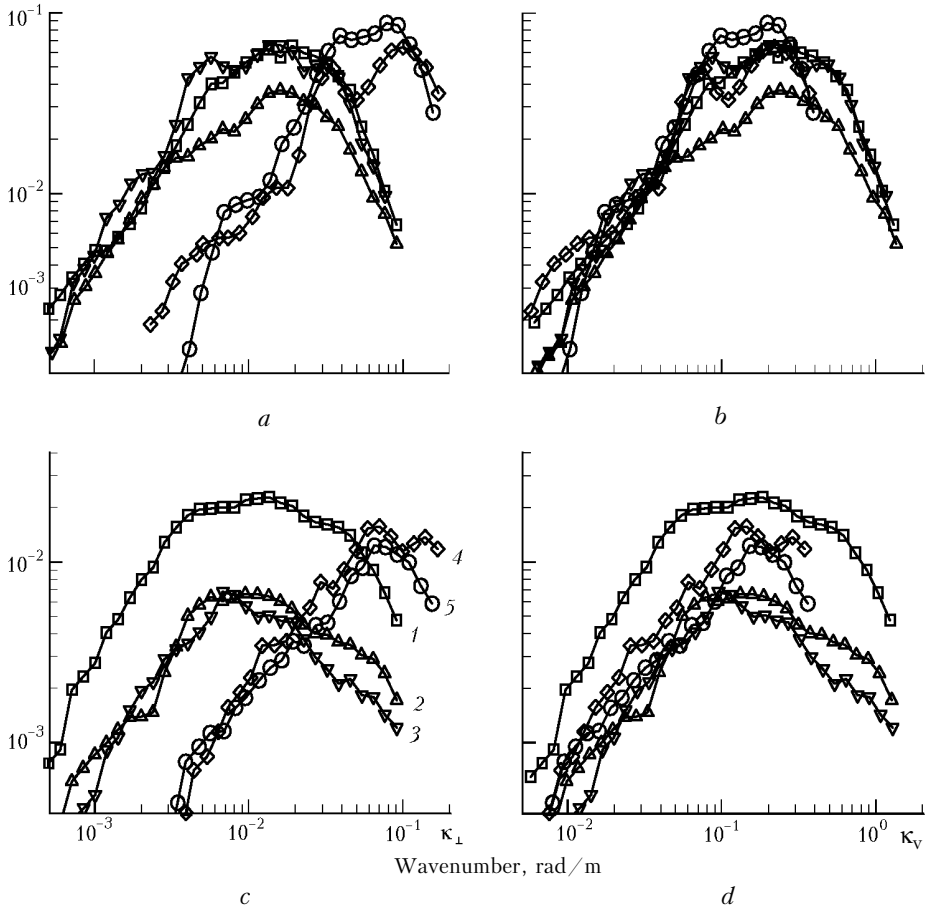

Fig. 4. Spatial scintillation spectra, obtained using hypothesis of isotropic inhomogeneities (*a*, *c*) and hypothesis of anisotropic inhomogeneities (*b*, *d*). Upper curves are calculated for heights 27–31 km, lower curves for heights 32–37 km. Curves *1* – *3* are for cases Nos. 25–27; curves *4* and *5* are for cases Nos. 32 and 31.

From Figs. 4*b* and *d* it is seen that the spectra $\kappa_v V_I(\kappa_v)$ are very similar in shape and have a maximum near some characteristic vertical scale $l_* = 2\pi/(\kappa_v)_{max} =$ = 30–60 m. We note that, in the case of purely power-law three-dimensional spectrum of the turbulent inhomogeneities (including anisotropic ones) of refractive index, the spectral maximum, in the meaning used here, must have been observed near the scale equal to the radius of the first Fresnel zone $\rho_F = \sqrt{2\pi\lambda L} \approx$ ≈ 2.5 m (Refs. 6–10), where L = 2100 km is the distance from perigee plane to the space station. In contrast, in the measurements the scintillations are attenuated starting from a scale l_*, which substantially exceeds ρ_F and, in this sense, it is interpreted as some internal scale for strongly anisotropic inhomogeneities. It must not be confused with the internal scale, usually used in the turbulence theory and associated with the molecular viscosity,[6] since the influence of molecular effects is too weak at these altitudes to cause a marked dissipation of kinetic turbulence energy on that large scales. Overall, the scintillation spectrum was the same in the altitude range from 25 to 36 km, with a characteristic scale l_* from a few tens to hundreds of meters.

As seen from Fig. 4, the scintillations in the data presented here are mainly caused by anisotropic inhomogeneities. Separation of isotropic Kolmogorov turbulence has not been possible in these measurements for the following reasons.

First, this is because the frequency range of the receiving system of the EFO-1 photometer was limited to about 100 Hz, whereas the maximum of scintillations caused by the isotropic Kolmogorov turbulence must have been observed at frequencies from one kilohertz to several kilohertzs (provided that the internal turbulence scale is less than the size of the Fresnel zone),[6] depending on the star set angle.

Second, for a weak fluctuation regime the influence of chromatism in the case of inclined star sets such as those realized in most of the experiments with EFO-1, leads not only to filtering out of isotropic scintillation in the high-frequency region, but also, and mostly, to a suppression of scintillations throughout the spectrum including large-scale region.[29,30] This is associated with the fact that, due to chromatism, the sensing radiation have different resolution, determined by the size of Fresnel zone ρ_F in horizontal and by chromatism scale Δh_c in the vertical. Even with the use of a narrowband filter F_1, the scale Δh_c becomes comparable with ρ_F already at heights 35–38 km, and then decreases roughly exponentially with the decreasing altitude in

altitude range of interest here. When the atmosphere is sensed nearly vertically, the chromatism leads to an effective smoothing out of scintillations with the scales less than Δh_c, for both anisotropic and isotropic inhomogeneities. At the inclined star sets, in case of anisotropic inhomogeneities, the chromatism effect is the same as at the vertical sensing. In the case of sensing the isotropic inhomogeneities (along the direction quite close to the horizon), the chromatism does not lead to a noticeable averaging of the high-frequency scintillations because the horizontal resolution of remote sensing is high and scintillation spectrum still has high frequencies. Since the variance of scintillations is an integral of the spectrum over all frequencies, and for this reason it does not depend on viewing direction, it seems reasonable to expect that for the slant viewing directions the spatial spectrum of isotropic scintillations (usually much broader than for vertical sensing) should have much lower spectral amplitudes.

These circumstances have led to the fact that, with the isotropic/anisotropic turbulence ratio observed in the atmosphere, the EFO-1 measurements failed to reveal, at altitudes below 35–38 km, the scintillations caused by the isotropic inhomogeneities. Underestimation of chromatism has led us in Ref. 14 to underestimated values of possible stratospheric values of the structure characteristics of temperature fluctuations for isotropic Kolmogorov turbulence. On the other hand, such a separation of the scintillations by the type of turbulent inhomogeneities has made it possible to thoroughly study the characteristics of anisotropic turbulence with the EFO-1 device, not specialized for tackling these tasks.

In a number of cases when scintillations were reliably fixed against the noise background, at altitudes above 40 km, where the selective chromatism effect was not that significant, qualitative changes in the shape of scintillation spectra, toward exhibiting poorly defined or no maximum at all, was observed. Such changes in scintillation spectra, typically occurring in the presence of isotropic turbulence against the background of anisotropic scintillations, were recorded in the cases Nos. 26–29, 31, 32, 34, 38, and 39. The scintillation spectra obtained in cases 38 and 39 can be found in Ref. 18.

Note that the chromatism in measurements considered here might also lead to underestimation of characteristic scale l_*, mentioned above, for altitudes below 30–35 km, where the chromatism effects are significant. The measurements carried out with a new photometer EFO-2,[25] in which filters with much narrower bandpass are applied, show that the characteristic scale l_* has a tendency to decrease with the decreasing height.

Precisely, the possibility of recording isotropic Kolmogorov turbulence in the experiment was the main motivation for the development of a new specialized EFO-2 photometer, whose main advantages over EFO-1 were faster operation, use of filters with a narrower bandpass, and larger receiving aperture. All this has made it possible to increase substantially the measurement resolution and to record reliably the scintillations caused by both anisotropic and isotropic turbulence.[24,25]

As seen from Fig. 4, the anisotropy of inhomogeneities was so large that, even for inclined star settings with $\alpha = 86°$, the inhomogeneities were crossed by the sensing ray in vertical. To study the horizontal structure of scintillations and obtain more accurate estimates of the anisotropy coefficient, we have performed measurements in which the star was observed near satellite orbital pole. In such observations, the star set down to minimum altitude h_{min} and then rose again. In these measurement series, the observations were made in successive orbits every 1.5 h; and from one orbit to another, the h_{min} value changed by several kilometers due to precession of the orbit. In the vicinity of the trajectory with the minimum height h_{min} the ray perigee moved practically along the horizon for a few hundred kilometers. The data obtained along these fragments of the trajectories were then used to calculate the horizontal scintillation spectra. The comparative analysis of vertical and horizontal scintillation spectra has made it possible to estimate the anisotropy coefficient of inhomogeneities to be $\eta \approx 160$ in the altitude range 22–30 km (Refs. 17 and 19).

6. Temperature fluctuation spectra in the stratosphere

As was already noted above, in the phase screen approximation for weak scintillation regime, simple relationships exist between two-dimensional spectra of phase fluctuations on a screen and measured scintillations, while the spectrum of phase is determined, in turn, by the three-dimensional spectrum of fluctuations of the refractive index in the atmosphere.[7–10,23] In the experiment, we measured the one-dimensional scintillation spectrum on some segment of the star setting trajectory. Reference 16 considers how quite a large set of one-dimensional scintillation spectra, obtained in different viewing geometries, can in principle be used to retrieve two-dimensional scintillation spectra, and then the three-dimensional fluctuation spectrum of the refractive index. However, implementation of such a solution is impractical nowadays.

In analysis of the spectra obtained, it was assumed that the spectrum of atmospheric inhomogeneities could be considered as a sum of isotropic and anisotropic components. The use of *a priori* information on the character of inhomogeneities in the refractive index, causing the observed scintillations, primarily concerning the strong anisotropy of these inhomogeneities, and the fact that the characteristic scale l_* is many times larger than the size of Fresnel zone, substantially simplifies the task. As analysis shows,[16] in this case one can obtain simple formulas relating the vertical scintillation spectrum with the vertical fluctuation spectrum of the refractive index or temperature.

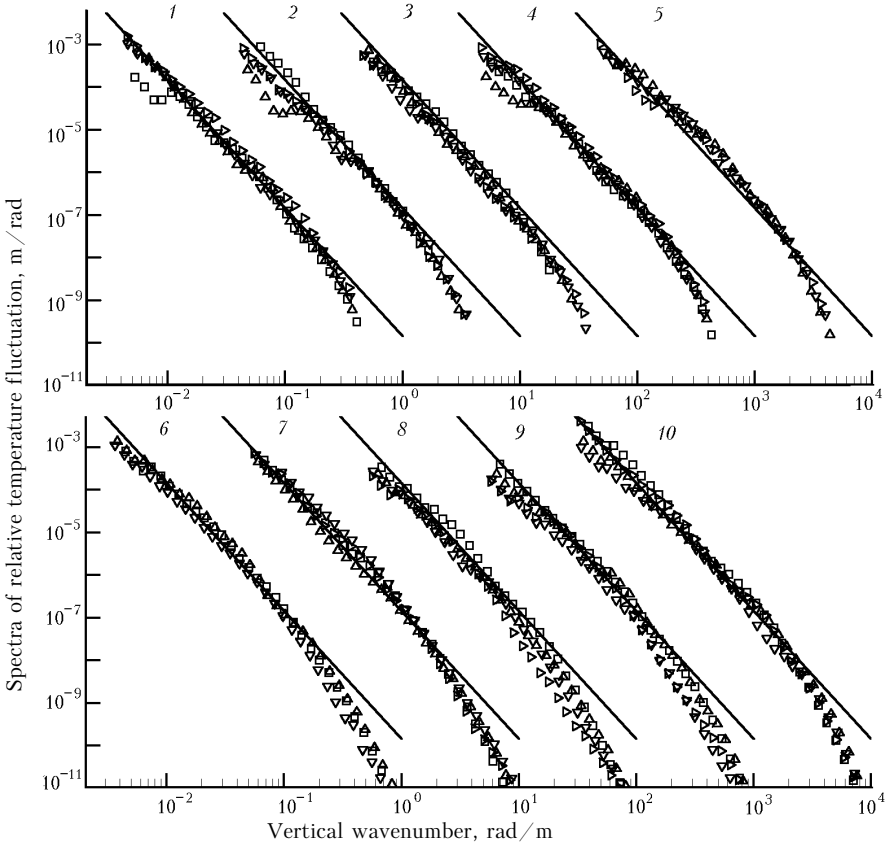

Fig. 5. Vertical spectra of relative temperature fluctuations: data of observations of Sirius set (curves *1–5*), cases 32, 28, 29, 31, 33; and of Canopus set (curves *6–10*), cases 16, 25–27, and 18. The spectra are orderly shifted by an order of magnitude along the abscissa axis. Different symbols are used to indicate the data obtained at different altitudes. Shown by straight lines is power-law spectrum with the slope −3.

Figure 5 shows the vertical spectra of relative temperature fluctuations $V_T(\kappa_v)$ retrieved from the measured scintillation spectra under assumption of strong anisotropy of the inhomogeneities.

The spectra are given for series of observations of Sirius and Canopus sets. The data refer to the altitude range 25–37 km. Each spectrum (starting from curve *2* in the upper plot, and starting from the curve *7* in the lower plot) is orderly shifted by an order of magnitude along the wave number axis. We underscore once more that scintillations in these observations were caused primarily by strongly anisotropic inhomogeneities, whereas influence of isotropic turbulence was strongly offset by chromatic aberration of the atmosphere.[30] For each of the star set, the straight lines correspond to the model of saturated internal gravity waves (IGW)[28] $V_T^m(\kappa_v) = A\varpi_{BV}^4/(g^2\,\kappa_v^3)$, where ϖ_{BV} is Brunt–Vaisala frequency and $\varpi_{BV} \approx 0.022$ rad/s for the standard conditions in the stratosphere; g is the acceleration of gravity; and A is the coefficient. Its value was 0.06 as an average over all spectra of temperature fluctuations we have obtained from the observations of scintillations.

The wide range (over eight orders of magnitude) of V_T variations, resulting, after their recalculation, from scintillation spectra, and the logarithmic scale of their representation mask somewhat the difference between the spectra pertaining to different altitudes and different sensing regions, though the spread of parameters might be considerable. A general look at the spectra reveals some common features. According to the dependence observed, the spectra are separated by the scale l_* into two parts. In the large-scale region from 1 km to 100 m, they behave as power-law ones with the slope close to −3, consistent with the model of saturated IGW. Analysis of all scintillation observation data shows that the values of spectral slopes in the large-scale region are mostly concentrated in the range from −2.6 to −3.2, with most probable value of −2.8. The coefficient A is also close to what the model of saturated IGW predicts: $A = 0.1$ (Refs. 28 and 31). In the region of scales below l_*, a steeper spectral falloff of the retrieved spectra is observed.

We have compared the vertical spectra of temperature fluctuations, retrieved from scintillation measurements, with the spectra obtained by French scientists form *in situ* balloon-borne measurements in the altitude range 22–30 km (at higher altitudes, the balloon-borne measurements were not performed).[32] The comparison has shown good agreement among the spectra in the large-scale region, and a disagreement for scales less than ~ 50 m. The reasons for such a disagreement seem to be as follows. The main reason, as was already

noted above, lies in the fact that in star setting observations, the chromatism selectively suppressed the scintillations on isotropic turbulence for inclined star sets. In contrast, during *in situ* measurements, both of the turbulence components were present. After the effect of chromatism in scintillation observations was minimized[25] with the new EFO-2 sensor, both components, anisotropic and isotropic, were observed in the scintillation spectrum for the inclined star sets. In addition, the balloon-borne temperature measurements are made along a local trajectory of balloon ascent; whereas in satellite observations, the scintillations are caused by all inhomogeneities distributed along the line-of-sight path passing throughout the atmosphere. In data analysis, the intermittency effects must also be taken into account.

Good agreement among the temperature spectra in the large-scale region may serve an indicator of the efficiency of remote-sensing study of the inhomogeneous structure of the stratosphere based on satellite observations of the stellar scintillations.

Conclusion

The analysis of EFO-1 measurements was primarily aimed at studying the small-scale structure of inhomogeneities in stratospheric density and temperature using data of stellar scintillation observations. The EFO-1 measurements have made it possible to detect and study the anisotropic inhomogeneities of density. In these measurements, we were unable to study the characteristics of isotropic Kolmogorov turbulence in the stratosphere, due to insufficient resolution of the sensor in the high-frequency region and masking of the isotropic scintillations by anisotropic ones in low-frequency region.

The main results obtained in the studies of the structure of anisotropic inhomogeneities, are the following:

it is shown that the inhomogeneities of density, strongly elongated in horizontal, are permanently present in the stratosphere, with the vertical scales from few tens of meters to a few kilometers;

the characteristic inhomogeneity anisotropy coefficient is obtained (~ 100);

the vertical spectra of temperature inhomogeneities in the stratosphere are retrieved, and main parameters of the temperature fluctuation spectra in the altitude range 24–36 km are estimated. In the region of vertical scales from 1–2 to 0.1 km, the spectra can be approximated by power-law dependence with slope –3. For this region, we obtained a satisfactory agreement with *in situ* balloon-borne fluctuation measurements and with the calculations based on the model of saturated internal waves. In the region of smaller vertical scales, the spectral density of anisotropic inhomogeneities falls off much faster;

at high altitudes (38 km and above), deviations in the behavior of scintillation spectra from the behavior noted earlier were observed, with less pronounced, or even no, spectrum decay in the small-scale region. This change in the spectra might be due to the appearance of isotropic turbulence at heights where influence of the chromatism effects is not that significant.

In addition to analysis of statistical characteristics of random inhomogeneities of density in the stratosphere, we performed a number of other studies based on star set observations.

a) In August 1991, we performed a series of observations aimed at studying attenuation of light in the stratospheric cloud from Pinatubo eruption in the tropical zone. The vertical optical depth of the volcanic cloud is estimated, and fine vertical cloud structure is studied.

b) In one of the observation series, at the heights of 52–54 km over the region with coordinates 27.4–22.7°N, 116.7–127.9°E, we recorded thin regions characterized by anomalously strong vertical temperature variations. In the layers 50–200 m thick, the lapse rate could range from 4 to –7 K/100 m.

c) A number of other anomalies in the behavior of the mean atmospheric transmission and in the character of observed scintillations was also noted; but they are still poorly understood.

The ten-year series of observations of stellar scintillations with an EFO-1 sensor from onboard of two orbital stations has made it possible to study the statistical characteristics of strongly anisotropic inhomogeneous structures of density in the stratosphere. Already first measurements performed have shown usefulness of these observations in remote monitoring of stratospheric turbulence, and laid a foundation for the development and design of new specialized photometer EFO-2.[24,25] With the new device, it has been possible not only to improve the quantitative characteristics of the obtained data and extend the studied altitude range up to 70 km, but also to address a new issue in terms of the possibility of analyzing the characteristics of anisotropic and isotropic turbulence and to study the relationship between them.

Acknowledgments

The authors of this paper express many thanks to scientific team which has ensured and conducted the experiments with EFO-1 photometer from onboard Salyut-7 and Mir space stations: the USSR space pilots V.V. Lebedev, V.A. Dzhanibekov, A.P. Aleksandrov, M.Kh. Manarov, Yu.V. Romanenko, V.G. Titov, A.A. Volkov, S.K. Krikalev, A.A. Serebrov, A.P. Artsebarskii, and "Energy" Rocket Space Complex personnel S.I. Serova and A.I. Nesterenko.

A.S. Gurvich and V. Kan thank the Russian Foundation for Basic Research for support via grant No. 00–05–64376. V. Kan also thanks the support from Russian Foundation for Basic Research through the grant No. 01–02–16213.

References

1. O.I. Yakovlev, *Cosmic Radio Physics* (Nauchnaya Kniga, Moscow, 1998), 432 pp.
2. W.B. Hubbard, B. Sicardy, et al., Astron. and Astrophys. **269**, 541–563 (1993).
3. G.M. Grechko, A.S. Gurvich, V. Kan, S.A. Savchenko, and S.V. Sokolovskii, J. Opt. Soc. Am. A **2**, No. 12, 2120–2123 (1985).
4. M.P. McCormick, Adv. Space Res. **7**, No. 2, 73–86 (1987).
5. V.A. Polyakov, Yu.M. Timofeev, A.S. Gurvich, V.V. Vorobiev, V. Kan, and J.-H. Yee, Izv. Ros. Akad. Nauk., Ser. Fiz. Atmos. Okeana **37**, No. 1, 56–66 (2001) (in print).
6. V.I. Tatarskii, *Wave Propagation in Turbulent Atmosphere* (Nauka, Moscow, 1967), 548 pp.
7. A.S Gurvich, Izv. Vyssh. Uchebn. Zaved., Ser. Radiofiz. **27**, No. 8, 951–959 (1984).
8. B.S. Haugstad, Radio Sci. **13**, No. 3, 435–440 (1978).
9. W.B. Hubbard, J.R. Jokipii, and B.A. Wilking, ICARUS **34**, No. 34, 374–395 (1978).
10. R. Woo, A. Ishimaru, and F.-Ch. Yang, Radio Sci. **15**, No. 3, 695–703 (1980).
11. A.S. Gurvich, I. Zakharov, V. Kan, V.V. Lebedev, A.I. Nesterenko, L. Neuzhil, A.I. Pakhomov, and S.A. Savchenko, Izv. Akad. Nauk SSSR, Ser. Fiz. Atmos. Okeana **21**, No. 12, 1235–1241 (1985).
12. L.V. Bogdanov, G.M. Grechko, A.S. Gurvich, V.A. Dzhanibekov, S.I. Evstafieva, V. Kan, A.I. Pakhomov, and S.A. Savchenko, Dokl. Akad. Nauk SSSR **295**, No. 2, 317–321 (1987).
13. G.M. Grechko, A.S Gurvich, V.A. Dzhanibekov, V. Kan, and S.A. Savchenko, Issled. Zemli iz Kosmosa, No. 4, 22–27 (1989).
14. A.P. Aleksandrov, G.M. Grechko, A.S. Gurvich, V. Kan, M.Kh. Manarov, A.I. Pakhomov, Yu.V. Romanenko, S.A. Savchenko, S.I. Serova, and V.G. Titov, Izv. Akad. Nauk SSSR, Ser. Fiz. Atmos. Okeana **26**, No. 1, 5–16 (1990).
15. A.S. Gurvich, Atm. Opt. **2**, No. 3, 188–193 (1989).
16. A.S. Gurvich, and V. Kan, Atm. Opt. **2**, No. 4, 277–281 (1989).
17. A.A. Volkov, G.M. Grechko, A.S. Gurvich, V. Kan, S.K. Krikalev, A.I. Pakhomov, and S.A. Savchenko, Atm. Opt. **3**, No. 8, 806–811 (1990).
18. G.M. Grechko, A.S. Gurvich, V. Kan, A.I. Pakhomov, S.A. Savchenko, and A.A. Serebrov, Izv. Ros. Akad. Nauk, Ser. Fiz. Atmos. Okeana **29**, No. 1, 5–10 (1993).
19. G.M. Grechko, A.S. Gurvich, V. Kan, S.V. Kireev, and S.A. Savchenko, Adv. Space Res. **12**, No. 10, 169–175 (1992).
20. A.P. Artsebarskii, M.E. Gracheva, G.M. Grechko, A.S. Gurvich, V. Kan, S.K. Krikalev, A.I. Pakhomov, and S.A. Savchenko, Izv. Ros. Akad. Nauk, Ser. Fiz. Atmos. Okeana **30**, No. 4, 508–512 (1994).
21. G.M. Grechko, A.S. Gurvich, V. Kan, A.I. Pakhomov, S.A. Savchenko, and A.A. Serebrov, Izv. Ros. Akad. Nauk, Ser. Fiz. Atmos. Okeana **32**, No. 6, 790–795 (1996).
22. A.S. Gurvich and V. Kan, Izv. Ros. Akad. Nauk, Ser. Fiz. Atmos. Okeana **33**, No. 3, 314–323 (1997).
23. G.M. Grechko, A.S. Gurvich, V. Kan, A.I. Pakhomov, Ya.P. Podvyazny, and S.A. Savchenko, Dokl. Ros. Akad. Nauk **357**, No. 5, 683–686 (1997).
24. A.S. Gurvich, V. Kan, S.A. Savchenko, A.I. Pakhomov, P.A. Borovikhin, O.N. Volkov, A.Yu. Kaleri, S.V. Avdeev, V.G. Korzun, G.I. Padalka, and Ya.P. Podvyazny, Izv. Ros. Akad. Nauk, Ser. Fiz. Atmos. Okeana **37**, No. 4, 469–486 (2001).
25. A.S. Gurvich, V. Kan, S.A. Savchenko, A.I. Pakhomov, and G.I. Padalka, Izv. Ros. Akad. Nauk Ser. Fiz. Atmos. Okeana **37**, No. 4 (2001) (in print).
26. S.M. Rytov, Yu.M. Kravtsov, and V.I. Tatarskii, *Introduction to Statistical Radio Physics.* Part 2. *Random Fields* (Nauka, Moscow, 1978), 463 pp.
27. G.M. Grechko, A.S. Gurvich, V.A. Kazbanov, M.S. Kiseleva, A.I. Lazarev, I.N. Reshetnikova, G.E. Sinel'nikova, and S.V. Sokolovskii, Tr. S.I. Vavilova State Optical Institute, No. 205, 3–120 (1989).
28. S.A. Smith, D.C. Fritts, and T.E. VanZandt, J. Atmos. Sci. **44**, No. 10, 1404–1410 (1987).
29. A.S. Gurvich and V.L. Brekhovskikh, *Waves Random Media* (accepted 2001).
30. V. Kan, F. Dalaudier, and A.S. Gurvich, Appl. Opt. **40**, No. 6, 878–889 (2001).
31. T. Tsuda, T.E. VanZandt, M. Mizumoto, S. Kato, and S. Fukao, J. Geophys. Res. D **96**, No. 9, 17265–17278 (1991).
32. F. Dalaudier, A.S. Gurvich, V. Kan, and C. Sidi, Adv. Space Res. **14**, No. 9, 61–64 (1994).